Neutron capture cross section of ^{139}La

S. O'Brien,* S. Dababneh,† M. Heil, F. Käppeler,‡ and R. Plag
Forschungszentrum Karlsruhe, Institut für Kernphysik, 76021 Karlsruhe, Germany

R. Reifarth
Los Alamos National Laboratory, Los Alamos, New Mexico 87545, USA

R. Gallino and M. Pignatari
Dipartimento di Fisica Generale, Università di Torino and Sezione INFN di Torino, Via P. Giuria 1, I-10125 Torino, Italy

The neutron capture cross section of ^{139}La has been measured relative to that of ^{197}Au by means of the activation method. The sample was irradiated in a quasistellar neutron spectrum for $kT = 25$ keV generated via the ^{7}Li$(p,n)^7$Be reaction with the proton energy adjusted 30 keV above the threshold. Maxwellian averaged neutron capture cross sections were calculated for energies $kT = 5-100$ keV. The new value for $kT = 30$ keV is found to be 31.6 ± 0.8 mb, 18% lower and considerably less uncertain than the previously recommended value of 38.4 ± 2.7 mb. With these results the *s*- and *r*-process components could be more accurately determined, making lanthanum a reliable *s*- and *r*-process indicator in stellar spectroscopy.

I. INTRODUCTION

Stellar nucleosynthesis models have been steadily improving since the concept of neutron capture reactions in stars as the origin of the heavy elements was established by Burbidge, Burbidge, Fowler, and Hoyle [1] and Cameron [2] four and a half decades ago. By postulating the *s* process as a sequence of neutron captures occurring on a slower time scale than the typical half-lives for β decay of unstable nuclides along the *s* path, this concept of the canonical *s* process has had a great deal of success in reproducing the observed *s*-process abundances in the universe. Current models, which have been built from the groundwork set forth by these seminal works, are moving ever closer to deciphering the physical conditions during *s*-process nucleosynthesis that occurs in thermally pulsing asymptotic giant branch (AGB) stars [3].

Isotopes with closed neutron shells, known as the neutron magic isotopes, are of special importance in the *s*-process reaction chain. Because of their very low (n,γ) cross sections, they act as bottlenecks in the chain of neutron capture reactions, in particular at neutron numbers $N = 50$, 82, and 126. Though difficult to measure, an accurate assessment of the cross sections at magic neutron numbers is important for the quantitative interpretation of the bottleneck effect in these regions. There are two main aspects of this effect, given as follows.

(i) These isotopes build up to large abundances, which are more easy to observe by stellar spectroscopy. Since their large *s* abundances dominate the respective *r*-process com-

ponents, they are therefore considered *s*-process indicators.

(ii) They also determine the shape of the overall *s*-process abundance distribution, which allows one to constrain the characteristic parameters of the stellar *s*-process site.

As far as the first aspect is concerned, lanthanum has the advantage that it is practically monoisotopic, since the second stable isotope ^{138}La contributes less than 0.1%. Hence, the solar *s*-process abundance of lanthanum can be defined by an accurate capture cross section of ^{139}La. Subtracting the *s* component from the total solar abundance will then also provide a reliable *r*-process abundance fraction, which is required, e.g., for characterizing the element patterns observed in very metal-poor stars [4]. On the spectroscopical side, La is well suited for studying the composition of stars which exhibit either *s*- or *r*-process enhanced atmospheres. This is true because La exhibits many clear but unsaturated spectral lines, for which accurate oscillator strengths gf have been reported recently [5]. On one hand, lanthanum is an *s*-process indicator of the $N = 82$ abundance peak, and represents together with barium, cerium, praseodymium, and neodymium the so-called *heavy-s* (hs) elements. Compared to the *light-s* or "ls" component, usually expressed by the strontium, yttrium, and zirconium abundances, the ls/hs ratio provides a measure of the total neutron exposure characterizing the heavy element abundance distributions produced in different *s*-enhanced stars. On the other hand, lanthanum becomes also the best indicator of the *r* process in metal-poor stars, which prevail at times when low-mass stars have not had time to evolve up to the AGB phase and to pollute the interstellar medium with *s*-process material. In these cases, the heavy elements show only their *r*-process component.

Since europium represents an element with dominating *r*-process abundances, the lanthanum/europium ratio provides a measure of the *s*- and *r*- process components in unevolved halo stars in the range $-2 < $[Fe/H]$ < -1$, showing the transition between the *r* and the *s* process in the galaxy [6]. (The spectroscopic notation is defined as [Fe/H]

---

*Permanent address: Department of Physics, University of Notre Dame, Notre Dame, IN 46556.

†On leave from Faculty of Applied Sciences, Al-Balqa Applied University, Salt 19117, Jordan.

‡Corresponding author. Email address: franz.kaeppeler@ik.fzk.de

= log(Fe/H)-log(Fe/H)$_\odot$.) Because of the difference in time scales of the *s* process, which is ascribed to He burning in slowly evolving low-mass stars, and the *r* process, which is ascribed to the supernova explosions of quickly evolving massive stars, the *s/r* ratio is an important key to understanding galactic chemical evolution of the heavy elements. Besides La, barium is also used to determine the hs component but barium lacks the advantage of being (nearly) monoisotopic such as lanthanum. Though easily observed spectroscopically, the analysis of the Ba lines suffers from saturation effects, hyperfine splitting, and uncertain *gf* values.

An example of these difficulties is the analysis of the very metal-poor star HD 140283 with [Fe/H]$=-2.4$. From the spectroscopic analysis of the line at 455.4 nm, its isotopic pattern of barium was first interpreted to exhibit a solar (*s* $+r$) composition [7], but then recently recognized as being of pure *r*-process origin [8]. Since it can be easily identified even in faint objects, lanthanum is a preferable alternative to use in such studies of the *s/r* ratio in old, metal-poor stars.

The importance of the second aspect refers, for example, to the average time-integrated neutron flux of the main *s*-process component, which describes the heavy *s*-process abundances in the mass range $90 \leq A \leq 209$ [9,10]. Of the isotopes with magic neutron number 82, only the effect of ^{142}Nd has been studied in sufficient detail [11]. A similar bottleneck effect in this mass region may also result from an improved ^{139}La cross section.

In spite of the spectroscopic advantages of lanthanum as a key element for characterizing both the *s* process and the *r* process in different classes of stars, the required accuracy of its neutron capture cross section is not adequately met at the present. The previously reported Maxwellian averaged cross sections at $kT=30$ keV show large discrepancies, with values ranging from 11.6 [12] to 50 mb [13]. This work is aimed at measuring the ^{139}La capture cross section with the necessary accuracy for a quantitative assessment of the physical conditions during nucleosynthesis in this important part of the *s*-process path. The following sections describe the measurement of the capture cross section of ^{139}La (Sec. II) and the data analysis procedure (Sec. III). Results and astrophysical implications are discussed in Secs. IV and V, respectively.

II. EXPERIMENTAL TECHNIQUE

The activation measurement on ^{139}La was carried out at the Karlsruhe 3.7-MV pulsed Van de Graaff accelerator. The neutron spectrum was produced via the ^{7}Li$(p,n)^7$Be reaction by bombarding a 30-μm-thick metallic lithium target of 6 mm diameter with protons of 1911 keV, 30 keV above the reaction threshold. The resulting neutron spectrum is a continuous distribution in neutron energy and has a high energy cutoff at $E_n=106$ keV. The reaction kinematics restrict the emitted neutrons to a forward cone with an opening angle of 120°. The angle integrated spectrum peaks at 30 keV and nearly reproduces a Maxwellian neutron spectrum with a thermal energy of $kT=25 \pm 0.5$ keV [14]. Hence, the reaction rate measured in such a spectrum represents the proper stellar cross section to very good approximation.

TABLE I. Summary of irradiation parameters.

Activation	Mass (mg)	Irradiation time (h)	Measuring time (h)	Flux divergence[a] (%)
LA1	12.40	22	24	20.5
LA2	11.92	47	10	11.2
LA3	12.63	17	22	2.9

[a]Calculated as the difference in the flux measured by the two gold foils divided by the average flux.

The samples were 7-mm-diameter disks that were cut from a metallic lanthanum foil of natural composition. The use of an additional lanthanum oxide sample was turned down, since the oxide (La$_2$O$_3$) and the hydroxide (La[OH]$_3$) form white powders, which makes it difficult to define the stoichiometry and thus the mass of lanthanum in the sample. Lanthanum is known to oxidize quickly in air. Therefore, the sample was polished and stored in an argon atmosphere in order to remove and prevent surface impurities.

For the irradiation, the lithium target was evaporated onto a 1-mm-thick, water cooled copper backing. The sample was then placed in close geometry with the lithium target such that the entire sample was inside the neutron cone. During the irradiation, lanthanum was again kept in an argon-filled container to prevent any oxidation during the experiment that may lead to sample deterioration and deformation. The measurement was carried out relative to ^{197}Au as a standard. To accomplish this, the sample was sandwiched between two gold foils, each having a diameter of 7 mm as well. Throughout the activation, the neutron yield was continuously monitored and recorded with a ^{6}Li-glass detector positioned 97 cm away from the target along the beam axis. The monitoring is needed in order to later correct for fluctuations of the neutron fluence (Sec. III).

The measurement consisted of three activations, therefore allowing the experimental parameters to be varied. The irradiation times ranged from 17 to 47 h, and the measuring times varied between 10 and 24 h. The most important parameter that was varied was the positioning of the gold foils relative to the lanthanum sample. This parameter is characterized by the flux divergence, which is calculated as the difference in the flux measured by the two gold foils divided by the average flux (Sec. III). The reason for varying the irradiation parameters was to study their effects on the measurement and the associated errors. The parameters of the irradiations are listed in Table I.

Following the irradiations, the induced activities of the gold foils and of the La sample were counted in a low background environment, using a 39-cm^3 high-purity Ge detector in a well defined geometry. The sample-detector distance of 76 mm was reproducible within ± 0.1 mm. Figure 1 shows the γ-ray spectrum emitted by the lanthanum sample during the 22 h measuring time following activation LA3. All features present in the diagram are attributed to the decay of ^{140}La, and the four γ-ray lines used in the analysis are indicated. Table II lists the decay parameters of these four lines,
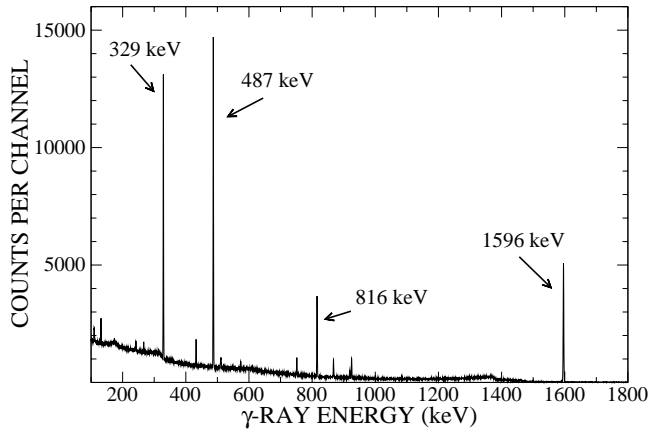
FIG. 1. The γ-ray spectrum emitted by the lanthanum sample after irradiation as measured by a germanium detector. The lines used in the analysis are indicated in the plot. Details of the irradiations are described in the text.

as well as the parameters of the γ-ray line used to analyze the gold foils.

III. DATA ANALYSIS

The net counts C_γ registered in the Ge detector for a given characteristic γ-ray line can be expressed as

$$C_\gamma = AK_\gamma \epsilon_\gamma I_\gamma f_w f_m S_\gamma, \qquad (1)$$

where A denotes the total number of activated nuclei at the end of irradiation, K_γ the correction factor for γ-ray self-absorption, ϵ_γ the efficiency of the Ge detector, and I_γ the γ-ray intensity per decay. The time factors $f_w = e^{-\lambda t_w}$ and $f_m = (1 - e^{-\lambda t_m})$, as discussed by Beer and Käppeler [15], account for the fraction of nuclei that decay during the waiting time t_w after irradiation and during the measurement time t_m; λ is the decay constant of the respective product nucleus. S_γ is the correction factor corresponding to the summing effects in the Ge crystal.

The corrections for γ-ray self-absorption K_γ were calculated with the absorption coefficients of Storm and Israel [16] listed in Table III. The correction factor for the summing effect in the Ge detector, S_γ, was explored by means of Monte Carlo simulations using the GEANT4 toolkit [17]. For this purpose the Ge crystal, with its dead layers and alumi-

TABLE II. Decay properties of the product nuclei.

Product nucleus	Half-life (d)	γ-ray energy [a] (keV)	Intensity per decay [a] (%)
^{140}La	1.6781 ± 0.0003	328.76	20.3 ± 0.3
		487.02	45.5 ± 0.6
		815.77	23.3 ± 0.2
		1596.2	95.4 ± 1.5
^{198}Au	2.6952 ± 0.0002	411.80	95.6 ± 0.1

[a]Data extracted from the NUDAT database, version 2002 [30].

TABLE III. Compilation of calculated correction factors.

Nucleus	γ-ray energy (keV)	Summing correction factor	Self-absorption factor
^{140}La	328.76	0.9824	0.997
	487.02	0.9898	0.998
	815.77	0.9997	0.999
	1596.2	0.9944	0.999
^{198}Au	411.80	1.0000	0.995

num housing, together with the lead shield and sample holder was carefully modeled. Monoenergetic γ rays corresponding to the four transitions under investigation were first generated in separate runs at the sample position and the energy deposited in the Ge crystal was histogrammed. The complex decay scheme of the ^{140}Ce levels was considered, including all transitions with intensities higher than 1% [18]. The summing correction factor for each γ transition was obtained by comparing the intensity of the line in the monoenergetic simulated spectrum to that in the complex decay spectrum. In all cases, the total number of generated events was 10^8. As expected, the summing effects were found to be small because of the small solid angle subtended by the detector. The summing corrections are given in Table III.

The total number of activated nuclei A is given by

$$A = \Phi_{tot} N \sigma f_b, \qquad (2)$$

where $\Phi_{tot} = \int \Phi(t) dt$ is the time-integrated neutron flux, N the number of sample atoms per cm^2, and σ the spectrum averaged neutron capture cross section. The correction factor f_b accounts for the variation of the neutron flux with time and corrects for the decay during activation [15]. The neutron flux is determined by the activation in the gold foils on both sides of the lanthanum sample via Eq. (2). The reference value chosen for the ^{197}Au cross section was 586 ± 8 mb, which was measured by Ratynski and Käppeler [14] using the same neutron spectrum. By averaging the induced activities of the gold foils, one is able to correct for target geometry, neutron scattering, and self-shielding. By combining Eqs. (1) and (2), and using the average neutron flux through the gold foils, one can calculate the sample cross section σ_{exp}.

IV. RESULTS AND DISCUSSION

The final ^{139}La(n,γ)^{140}La cross section was adopted from the result of the third activation with the smallest systematic uncertainty: $\sigma_{expt.} = 33.2 \pm 0.7$ mb. Throughout the analysis, the four strongest lines (Table II) of the decay of ^{140}La were studied. Though their intensities were found to be perfectly consistent with each other, only the line at 487 keV was considered for the final analysis. This line was chosen because it is the closest in energy to the 411.8-keV line of gold that was used to determine the neutron flux, and therefore any systematic deviation in the efficiency calibration of the

TABLE IV. Compilation of uncertainties.

Source of uncertainty	Uncertainty (%)	
	Au	La
Gold cross section[a]	1.5	
Sample thickness	0.1	0.2
Time factors f_w, f_m, f_b	Negligible	Negligible
Counting Statistics[b]	0.5	0.4
Self-absorption[b]	<0.05	<0.03
Detector efficiency ratio[b]		1.4
γ-ray intensity per decay[b]	0.5	1.3
Divergence of neutron flux[c]		0.7
Combined total uncertainties		2.2

[a]The uncertainty of the gold reference cross section is not included in the final uncertainty since it cancels out in most applications of relevance for nuclear astrophysics.
[b]The uncertainties are specific to the 411.8 and 487.0 keV γ-ray lines of gold and lanthanum, respectively.
[c]Estimated as 25% of the flux difference measured with the two gold foils.

Ge detector would have the smallest effect on the calculation of the cross section.

The experimental uncertainties are summarized in Table IV. The values listed for lanthanum are specific to the 487-keV line, but the uncertainties are representative of all the lines studied. For a comparison, Table V shows the computed cross sections that were calculated using each of the four lines in the γ-ray spectrum following the third activation. Also listed are the cross sections that resulted from the analysis of the 487-keV line in the γ-ray spectra of the first two irradiations.

Besides the gold cross section, another significant uncertainty arises from the detector efficiency. This uncertainty was calculated from the error band of the fitted detector efficiency, and is limited by the activity uncertainties of the calibration sources. The uncertainties introduced by the relative γ-ray intensities are also significant. This contribution might be reduced by future improvements of these values. The uncertainty in neutron flux at the position of the sample was estimated to be 25% of the difference between the two flux values measured with the gold foils. In the first two activations, it was found that this error dominated the overall

TABLE V. Cross sections obtained in activations 1–3 and by analyzing the different γ-ray lines measured in activation 3.

Activation	γ-ray energy (keV)	Cross section (mb)
LA1	487.02	35.3±1.9
LA2	487.02	33.3±1.2
LA3	487.02	33.2±0.7[a]
LA3	328.76	33.1±0.9
LA3	815.77	32.6±0.7
LA3	1596.80	32.4±0.9

[a]Adopted cross section (see text).

uncertainty. Therefore, in the third activation, the gold foils were placed as close to the sample as possible to reduce the difference in flux between the gold foils and correspondingly the associated uncertainty. The uncertainties in the time factors, which would arise from the uncertainties in the half-lives of the product nuclei and in the waiting and measuring times, were negligible.

The results obtained in the different activations and from analyzing the various γ-ray lines of ^{140}La are well compatible with the uncertainties listed in Table IV, thus confirming that systematic effects had been properly corrected.

In an astrophysical environment the neutron spectrum corresponds to a Maxwellian energy distribution

$$\Phi \sim E_n e^{-E_n/kT}. \tag{3}$$

Since the experimental neutron spectrum is similar in shape to a Maxwellian distribution with $kT = 25$ keV, the measured cross section represents a good approximation for this thermal energy. But because ^{139}La is a neutron magic nucleus, the energy dependence of its neutron capture cross section may well be different from that of the gold standard. In that case a correction for the cutoff energy in the experimental spectrum at 106 keV [14] has to be applied before the cross section can be used in an astrophysical context. The first step was to normalize the cross section provided online by the NEA Joint Evaluated Project in the Joint Evaluated File (JEF) [19] to the present result. The evaluated cross section was preferred over the statistical model calculation used in Ref. [20] since it considered the available experimental information on the energy dependence explicitly. To obtain the Maxwellian averaged cross section $\langle\sigma v\rangle/v_T$, the normalized cross section vs neutron energy was folded with a Maxwellian distribution according to the definition

$$\frac{\langle\sigma v\rangle}{v_T} = \frac{2}{\sqrt{\pi}} \frac{\int_0^\infty \sigma(E_n) E_n e^{-E_n/kT} dE_n}{\int_0^\infty E_n e^{-E_n/kT} dE_n}, \tag{4}$$

where $\sigma(E_n)$ is the differential cross section and E_n the neutron energy [14].

Assuming a 10% uncertainty for the corresponding correction, one obtains $\langle\sigma v\rangle/v_T = 35.7 \pm 0.8$ mb for the Maxwellian average at $kT = 25$ keV.

Starting from this result, the normalized cross section can now be used for determining the Maxwellian averages for the entire range of s-process scenarios, covering the temperature range from a few keV up to 100 keV. This wide range of temperatures [20] is required for describing all possible scenarios, including the advanced hydrostatic nucleosynthetic phases in massive stars and the explosive nucleosynthesis taking place during a supernova explosion [21]. The temperatures typical of the main s-process component, related to He shell burning in thermally pulsing low-mass AGB stars, are particularly important in this respect [22–24] (see Sec. V).

The Maxwellian averaged cross sections are given in column 2 of Table VI. In order to calculate the respective un-

TABLE VI. Maxwellian averaged ^{139}La cross sections.

Thermal energy (keV)	$\langle \sigma v \rangle / v_T$ (mb)[a]	
	Temperature trend from Ref. [19]	Temperature trend from Ref. [20]
5	104.0	96.1
8	76.3	70.1
10	65.8	60.4
15	50.0	47.6
20	41.3	40.8
23	37.7	37.5
25	35.7 ± 0.8	35.7 ± 0.8
30	31.6 ± 0.8	32.6
40	26.0	28.1
50	22.4	25.5
60	19.8	23.8
80	16.3	22.1
100	14.1	20.4

[a]Based on the experimental result of this work.

TABLE VII. s-process yields and r-process residuals.

Isotope	Abundance (relative to Si = 10^6)		
	Solar	s process	r process
^{133}Cs	3.72×10^{-1}	$5.39 \times 10^{-2} \pm 7.0\%$	$3.18 \times 10^{-1} \pm 6.7\%$
^{135}Ba	2.96×10^{-1}	$7.75 \times 10^{-2} \pm 7.1\%$	$2.19 \times 10^{-1} \pm 8.9\%$
^{137}Ba	5.04×10^{-1}	$3.30 \times 10^{-1} \pm 7.3\%$	$1.74 \times 10^{-1} \pm 23.0\%$
^{139}La[a]	4.46×10^{-1}	$\mathbf{3.26 \times 10^{-1} \pm 2.7\%}$	$\mathbf{1.20 \times 10^{-1} \pm 10.4\%}$
^{139}La[b]		$2.77 \times 10^{-1} \pm 7.3\%$	$1.69 \times 10^{-1} \pm 13.1\%$
^{141}Pr	1.67×10^{-1}	$8.13 \times 10^{-2} \pm 2.7\%$	$8.57 \times 10^{-2} \pm 5.3\%$
^{143}Nd	1.00×10^{-1}	$3.16 \times 10^{-2} \pm 1.9\%$	$6.84 \times 10^{-2} \pm 2.1\%$
^{145}Nd	6.87×10^{-2}	$1.89 \times 10^{-2} \pm 1.7\%$	$4.98 \times 10^{-2} \pm 1.9\%$
^{147}Sm	3.99×10^{-2}	$8.25 \times 10^{-3} \pm 1.7\%$	$3.17 \times 10^{-2} \pm 1.7\%$

[a]This experiment.
[b]Obtained with previous ^{139}La cross section [11].

certainties, one would need the error in the differential cross section, which is not provided in the evaluation [19]. Therefore, any additional errors are omitted except for the 25-keV value and for the value at 30 keV, which is commonly used for comparison of astrophysical (n, γ) rates. For the extrapolation from 25 to 30 keV an additional systematic uncertainty of 1.2% was considered. In column 3 of Table VI we have listed the Maxwellian averaged cross sections obtained with the temperature trend from the statistical model code NON-SMOKER [25] as quoted in Ref. [20]. Both trends deviate from a $1/v$ behavior, which would predict a Maxwellian averaged cross section at $kT = 5$ keV of 80 mb, whereas the JEF evaluation and the statistical model yield 104 mb and 96 mb, respectively.

The calculated Maxwellian averaged cross section at $kT = 30$ keV is 31.6 ± 0.8 mb, significantly smaller than the recommended value of 38.4 ± 2.7 mb [20] adopted from an earlier activation [26]. Compared with other previous measurements, the present result is found in agreement with, but much more precise than, the 28 ± 3.1 mb value reported in Ref. [27]. Of the rather uncertain experimental results reported prior to 1980, only the 26.5 ± 8 mb value of Ref. [28] is compatible with the present value, while no agreement within the uncertainties is found in the remaining cases [13,12,29].

V. ASTROPHYSICAL IMPLICATIONS

With the present Maxwellian averaged cross sections of ^{139}La, an s-process analysis has been performed using stellar models for thermally pulsing low-mass AGB stars [22]. This scenario describes the main s component in the mass range $90 < A < 204$ and is characterized by the subsequent operation of two neutron sources during a series of helium shell flashes. First, the ^{13}C$(\alpha, n)^{16}$O reaction occurs under radiative conditions during the intervals between convective thermal pulses. While the ^{13}C reaction provides most of the neu-

tron exposure at low temperatures ($kT \sim 8$ keV) and low neutron densities ($n_n \lesssim 10^7$ cm^{-3}), the resulting abundances are modified by a second burst of neutrons from the ^{22}Ne$(\alpha, n)^{25}$Mg reaction, which is marginally activated during the next convective instability, when high peak neutron densities of $n_n \gtrsim 10^{10}$ cm^{-3} are reached at $kT \sim 23$ keV. Although this second neutron burst accounts only for a few percent of the total neutron exposure, it is essential for adjusting the final abundance patterns of the s-process branchings. However, since ^{139}La is an unbranched isotope with a comparably small cross section, it is only marginally affected by the small exposure contributed by the ^{22}Ne neutron source, and its abundance changes only by a few percent during this high temperature phase.

AGB models were found to exhibit remarkably similar conditions for a range of stellar masses ($1.5 \leq M/M_\odot \leq 3$) and metallicities ($-0.4 \leq$ [Fe/H] ≤ 0). The actual efficiency for neutron capture nucleosynthesis depends on metallicity, on the choice of the amount of ^{13}C that is burnt, and on its profile in the intershell region, i.e., what has become known as the ^{13}C *pocket* [3]. Since the formation of this pocket is difficult to describe in a self-consistent way, current calculations of AGB nucleosynthesis have still to be based on a plausible parametrization. The calculations [11] and their present update based on the new La cross sections refer to the average of models for $1.5M_\odot$ and $3M_\odot$, a metallicity $0.5Z_\odot$, and the standard ^{13}C pocket [3,24], which has been shown to match the solar main s-process component fairly well.

The main result of the new cross sections is that the s component of the lanthanum abundance predicted by these calculations increases from 62% to 73%. This implies that lanthanum is an even better s-process indicator than had originally been thought. It was found that the improved cross section affected only the abundance of ^{139}La itself without any noticeable effect on the abundances of the following isotopes in the neutron capture chain, in contrast to a feature observed for the case of ^{142}Nd [11].

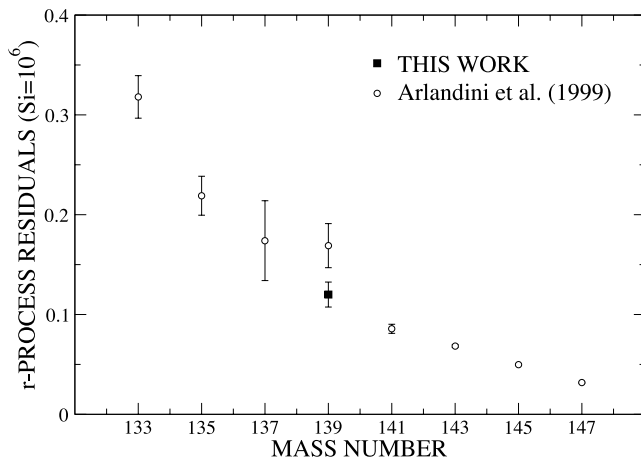The calculated s component of ^{139}La exhibits a clear dependence on the different choices of the temperature trends

FIG. 2. The *r* residuals in the $A = 139$ mass region. The new result for ^{139}La (solid square) is in better agreement with the smooth trend of the neighboring odd isotopes than the previous ^{139}La value.

of the Maxwellian averaged cross sections. If the Maxwellian averaged cross sections listed in column 3 of Table VI are used in the stellar model calculations, the *s*-component of the lanthanum abundance increases to 77%. This 4% difference is due to the different cross section shape vs neutron energy obtained with the JEF evaluation [19] and with the one provided by the statistical model [20]. This remaining discrepancy calls for an accurate measurement of the differential cross section, which is currently planned at the n-TOF facility at CERN via the time-of-flight method. This project will complement the present activation measurement to provide more complete data for an accurate assessment of the Maxwellian averaged cross sections at all relevant *s*-process temperatures.

From the revised *s* abundance of ^{139}La the corresponding improvement of the *r*-process contribution can be defined as the difference from the solar abundance, $N_r = N_\odot - N_s$. This expression, which neglects a possible but, in this mass region, small *p*-process contribution, was used to obtain the *r* abundances of the odd isotopes in the mass region around ^{139}La listed in Table VII. The corresponding plot (Fig. 2) illustrates that the new *r* abundance of ^{139}La fits the smooth

trend of the neighboring isotopes much better than the previous value.

In terms of the classical *s*-process approach, the present result would imply an increase of the solar *s* component of ^{139}La to slightly more than 100% compared with the 83% obtained with the previous value [11]. This solution is clearly ruled out, since it contradicts any plausible *r*-process expectation.

VI. SUMMARY

The stellar neutron capture cross section of ^{139}La has been measured via the activation method for 25 keV thermal energy. In total, three activations were performed to verify the corrections for various systematic uncertainties, thus providing a much better accuracy in the determination of the Maxwellian averaged cross section with a four times smaller uncertainty than that assigned to the previously recommended value [20]. The present result allowed us to resolve the persisting discrepancy in the data reported from different experiments. Based on the updated cross section, the *s* abundance component of ^{139}La could be determined with a clearly improved accuracy of 3%. Consequently, the *r* component can be defined with an uncertainty of 10% although its relative contribution was considerably reduced. This result makes lanthanum an even better *s*- and *r*-process indicator for stellar spectroscopy, defining the *r*-process abundance patterns in old, metal-poor stars in the transition from *r*- to *s*-process enrichments during galactic evolution and constraining the neutron exposures reflected in spectroscopic observations of carbon-rich and *s*-enhanced evolved stars.

[1] E. Burbidge, G. Burbidge, W. Fowler, and F. Hoyle, Rev. Mod. Phys. **29**, 547 (1957).

[2] A. Cameron, AECL Report CRL-41, 1957.

[3] R. Gallino *et al.*, Astrophys. J. **497**, 388 (1998).

[4] J.W. Truran, J.J. Cowan, C.A. Pilachowski, and C. Sneden, Publ. Astron. Soc. Pac. **114**, 1293 (2002).

[5] J.E. Lawler, G. Bonvallet, and C. Sneden, Astrophys. J. **556**, 452 (2001).

[6] D. Burris, C. Pilachowski, T. Armandroff, C. Sneden, J. Cowan, and H. Roe, Astrophys. J. **544**, 302 (2000).

[7] P. Magain, Astron. Astrophys. **297**, 686 (1995).

[8] D. Lambert and C. Allende Prieto, Mon. Not. R. Astron. Soc. **335**, 325 (2002).

[9] H. Beer, G. Walter, R. Macklin, and P. Patchett, Phys. Rev. C **30**, 464 (1984).

[10] F. Käppeler, Prog. Part. Nucl. Phys. **43**, 419 (1999).

[11] C. Arlandini *et al.*, Astrophys. J. **525**, 886 (1999).

[12] S. Chaturvedi and R. Prasad, in *Proceedings of the 15th Nuclear Physics and Solid State Physics Symposium* (Dept. of Atomic Energy, Bombay, 1971), Vol. 2, p. 615.

[13] A. de L. Musgrove, B. Allen, J. Boldeman, and R. Macklin, Australian Atomic Energy Commission, Report AAEC/E401, 1977.

[14] W. Ratynski and F. Käppeler, Phys. Rev. C **37**, 595 (1988).

[15] H. Beer and F. Käppeler, Phys. Rev. C **21**, 534 (1980).

[16] E. Storm and H. Israel, Nucl. Data Tables **7**, 565 (1970).

[17] See CERN, GEANT home page, Vol. 50A, http://wwwinfo.cern.ch/asd/geant4/geant4.html

[18] R. Firestone, in *Table of Isotopes*, edited by V. Shirley (Wiley, New York, 1996).

[19] C. Nordborg and M. Salvatores, in *Nuclear Data for Science and Technology*, edited by J. Dickens (American Nuclear Society, La Grange Park, 1994), p. 680.

[20] Z. Bao *et al.*, At. Data Nucl. Data Tables **76**, 70 (2000).

[21] T. Rauscher, A. Heger, R. Hoffman, and S. Woosley, Astrophys. J. **576**, 323 (2002).

[22] O. Straniero *et al.*, Astrophys. J. **440**, L85 (1995).

[23] O. Straniero *et al.*, Astrophys. J. **478**, 332 (1997).

[24] M. Busso, R. Gallino, and G. Wasserburg, Annu. Rev. Astron. Astrophys. **37**, 239 (1999).

[25] T. Rauscher and F.-K. Thielemann, At. Data Nucl. Data Tables **75**, 1 (2000).

[26] H. Beer, in *Advances in Nuclear Astrophysics*, edited by E. Vangioni-Flam *et al.* (Editions Frontières, Paris, 1986), p. 375.

[27] Y. Xia *et al.*, Chin. J. Nucl. Phys. **12**, 261 (1990).

[28] R. Anand, M. Jhingan, D. Bhattacharya, and E. Kondaiah, Nuovo Cimento A **50**, 247 (1979).

[29] A. de L. Musgrove, B. Allen, J. Boldeman, and R. Macklin, in *Neutron Physics and Nuclear Data for Reactors and Other Applied Purposes* (OECD, Paris, 1978), p. 449.

[30] R. R. Kinsey *et al.*, in *Capture Gamma-Ray Spectroscopy and Related Topics*, edited by G. Molnar, T. Belgya, and Z. Révay (Springer, Berlin, 1997), p. 657. Data extracted from the NUDAT database, version 2.5, 1996, http://www.nndc.bnl.gov/nndc/nudat/